Hierarchical Morphogenesis of Swallowtail Butterfly Wing Scale Nanostructures

Kwi Shan Seah[1,2] and Vinodkumar Saranathan*[1-5]

Affiliations:

[1]Division of Science, Yale-NUS College, 10 College Avenue West, 138609, Singapore.

[2]Department of Biological Science, National University of Singapore, 117543, Singapore.

[3]NUS Nanoscience and Nanotechnology Initiative (NUSNNI-NanoCore), National University of Singapore, 117581, Singapore.

[4]Lee Kong Chian Natural History Museum, National University of Singapore, 117377, Singapore.

[5]Present Address: Division of Sciences, School of Interwoven Arts and Sciences, Krea University, 5655, Central Expressway, Sri City, Andhra Pradesh 517646, India.

*E-mail : Vinodkumar.Saranathan@aya.yale.edu

Orcid IDs: KSS: 0000-0001-8451-3732; VS: 0000-0003-4058-5093

Abstract:

The study of color patterns in the animal integument is a fundamental question in biology, with many lepidopteran species being exemplary models in this endeavor due to their relative simplicity and elegance. While significant advances have been made in unravelling the cellular and molecular basis of lepidopteran pigmentary coloration,

the morphogenesis of wing scale nanostructures involved in structural color production is not well understood. Contemporary research in this topic largely focuses on a few nymphalid model taxa (*e.g.*, *Bicyclus*, *Heliconius*), despite an overwhelming diversity in the hierarchical nanostructural organization of lepidopteran wing scales. Here, we present a time-resolved, comparative developmental study of hierarchical scale nanostructures in *Parides eurimedes* and five other papilionid species. Our results uphold the putative conserved role of F-actin bundles in acting as spacers between developing ridges, as previously documented in several nymphalid species. Interestingly, while ridges are developing in *P. eurimedes*, plasma membrane manifests irregular mesh-like crossribs characteristic of Papilionidae, which delineate the accretion of cuticle into rows of planar disks in between ridges. Once the ridges have grown, disintegrating F-actin bundles appear to reorganize into a network that supports the invagination of plasma membrane underlying the disks, subsequently forming an extruded honeycomb lattice. Our results uncover a previously undocumented role for F-actin in the morphogenesis of complex wing scale nanostructures, likely specific to Papilionidae.

Key Words: Butterfly Scale, Biological Nanostructure, Hierarchical Morphogenesis, Structural Coloration, F-Actin Reorganization, Plasma Membrane Invagination

Introduction

The patterning and coloration of butterfly wings have been a paradigmatic research focus due to their fundamental role in signalling and crypsis (Beldade and Brakefield, 2002; Sweeney et al., 2003; Tsai et al., 2020). Significant advances have been made recently in identifying the cellular and molecular basis of lepidopteran pigmentary coloration (Matsuoka and Monteiro, 2018; Nadeau et al., 2016; Nishikawa et al., 2015; Reed et al., 2011; Van Belleghem et al., 2023; Zhang et al., 2017a). A small number of regulatory genes have been found to exert significant influence on the synthesis and spatial expression of pigments, as well as regulating cuticle deposition, thereby affecting the overall scale morphology (e.g., Banerjee et al., 2022; Brien et al., 2022; Ficarrotta et al., 2022; Matsuoka and Monteiro, 2018; Prakash et al., 2022; Van Belleghem et al., 2023; Wee et al., 2022). For instance, suppression of the *optix* gene has been found to tune lower lamina thickness, inducing iridescent structural coloration and affecting cuticular coverage of the upper lamina (Wasik et al., 2014; Zhang et al., 2017b).

Building on the classic studies on cellular organization of lepidopteran scales (Ghiradella, 1974; Ghiradella, 1985; Ghiradella, 1989; Ghiradella and Radigan, 1976; Overton 1966), a few recent studies utilized advances in microscopy techniques to interrogate the formation of longitudinal ridges (Day et al., 2019; Dinwiddie et al., 2014; McDougal et al., 2021). These insights are, however, limited to ridge formation on the scale surface. Moreover, contemporary research on scale cell development focuses on just a few model taxa (*Bicyclus*, *Precis*, *Heliconius*, *Vanessa*) all from the family of Nymphalidae (Beldade and Brakefield, 2002; Brien et al., 2022; Day et al., 2019; Dinwiddie et al., 2014; Matsuoka and Monteiro, 2018; Nadeau et al., 2016; Pomerantz et al., 2020; Prakash et al., 2021; Reed et al., 2011; Sweeney et al., 2003; Van

Belleghem et al., 2023; Wasik et al., 2014; Zhang et al., 2017b), despite an overwhelming diversity in the hierarchical organization of scale nanostructures across Lepidoptera (Ghiradella, 1984; Ghiradella, 1985; Ghiradella, 1989; Prum et al., 2006). A rare exception is the recent work on pierid butterfly *Colias* identifying *bric à brac* as a genetic switch that suppresses UV-reflecting Christmas-tree like ridge gratings in males (Ficarrotta et al., 2022), even though the precise development of the ridge grating is still unresolved (Ghiradella, 1974). Deciphering the cellular and developmental basis of scale organization in beyond just a few model lepidopterans is also highly relevant to current challenges in the synthesis of complex sub-micron and micron-scale hierarchical nanostructures, and could inspire novel biomimetic routes to fabricate multifunctional nanomaterials (Kolle et al., 2010; McDougal et al., 2019; Pokroy et al., 2009; Potyrailo et al., 2007; Siddique et al., 2017; Wilts et al., 2019).

The *bauplan* of lepidopteran wing scales consists an ornamented upper lamina over a relatively unstructured basal lamina, supported by arches with pillar-like struts called trabeculae (Ghiradella, 1984) (Fig. S1). The upper lamina comprised of longitudinal ridges with transverse crossribs framing a set of rectilinear windows. These windows typically open into the interior lumen of the scale cell, but can also be covered by a thin layer of cuticular lamina (Ghiradella, 1984). The sides of the ridges feature microribs – fine flute-like stripes visible at higher magnifications under an electron microscope (Fig. S1).

Among all Lepidoptera families, swallowtail butterflies (Papilionidae) not only encompasses the known diversity of scale nanostructure, but also exhibits some of the most complex hierarchical morphologies found in nature (Ghiradella, 1984; Ghiradella, 1985; Ghiradella, 1989; Prum et al., 2006; Saranathan et al., 2010) (Fig.

96 S1). Despite having a few model species (*e.g.*, *Papilio xuthus*, *P. polytes* and *P.*
97 *machaon*), the focus of current research on papilionids is limited to molecular basis of
98 mimicry of pigment patterns (e.g., Nishikawa et al., 2015; Yoda et al., 2021). The wing
99 scales of papilionid species (*e.g.*, *Parides sesostris*, *Papilio nireus*) exhibit irregular
100 veins or mesh-like crossribs, often with an underlying honeycomb-like lattice of
101 cuticular walls enclosing columnar pores (Ghiradella, 1984; Ghiradella, 1985;
102 Ghiradella and Radigan, 1976; Prum et al., 2006; Saranathan et al., 2010; Wilts et al.,
103 2014) (Figs. 1, and S1). In the following, we use "honeycomb lattices" to refer to
104 irregular crossribs with lattice walls extending into the interior lumen (*e.g.,* green
105 scales in *P. sesostris*, *P. arcas* and *P. eurimedes*), and "irregular crossribs" for
106 crossribs that lack such extruded cuticular walls. In any case, these irregular crossribs
107 are an autapomorphy of Papilionid butterflies (Ghiradella, 1984; Ghiradella, 1985;
108 Ghiradella and Radigan, 1976) that are thought to increase the surface area over
109 which pigments such as papiliochromes can be deposited (Wilts et al., 2012), and
110 likely play a role in thermoregulation as they are efficient absorbers of solar radiation
111 (Siddique et al., 2017).

112 Here, we use scanning electron microscopy (SEM), conventional confocal and
113 super-resolution Structured Illumination Microscopy (3D-SIM) to study the time-
114 resolved development of hierarchical scale nanostructures in wing scales of six
115 papilionid species, focusing mainly on *Parides eurimedes*. We discovered that
116 following ridge formation, rows of chitinous disks form in between the ridges, followed
117 by disintegration of F-actin that reorganizes into a mesh-like network. This network
118 likely acts as a template for subsequent formation of honeycomb lattices by driving
119 plasma membrane invagination into the scale lumen. Our study uncovers a novel
120 process of wing scale nanostructure formation in Papilionid species.

121

122 **Results**

123 *Wing scale ridge formation is conserved in Papilionidae*

124 We comparatively studied the wing scale growth in *Papilio polytes* and *Parides*
125 *eurimedes,* which have irregular crossribs and honeycomb lattices respectively. Early
126 stages of scale cell growth are as previously documented in several nymphalid
127 species (Day et al., 2019; Dinwiddie et al., 2014; Ghiradella, 1974; Pomerantz et al.,
128 2020). Wheat germ agglutinin (WGA) stains the plasma membrane during early
129 stages of scale development in *P. eurimedes*. Scale cells from relatively young pupae
130 at 38% development resemble elongated buds containing densely packed
131 polymerizing F-actin filaments (Fig. S2A-A'' and B-B''). At 43% development, F-actin
132 filaments form thicker bundles that extend down the full length of scale cells (Fig.
133 S2C'), laying down a scaffold that determines the eventual position of ridges
134 (Dinwiddie et al., 2014). WGA stains pleating membranes (longitudinal striations) in
135 between adjacent rows of F-actin bundles (Fig. S2C-C'' and D-D''). Around 48% to
136 50% development, the developing ridges can be more clearly discerned in between
137 F-actin bundles (Fig. S2E-E'', S15D-D'' and E-E''). At this stage, there also appears to
138 be irregular gaps in WGA staining in between the ridges of *P. eurimedes* scales (Fig.
139 S2E). These vein-like features resemble the irregular crossribs seen in adult wing
140 scales (Fig. 1B-C, Fig. S15B-C).

141

142 *Cross-rib and cuticular disk formation in Parides eurimedes*

143 We use lectin and membrane stains to follow plasma membrane topology and
144 cuticle deposition during scale cell maturation (Figs. 2, and S3-S6). At 48%
145 development, plasma membrane appears mottled while WGA predominantly stains

146 longitudinal striations that will become ridges (Figs. 2A-C, and S3B-B"). In cross-
147 sections, both stains appear to be in close contact at the periphery of the cell, with
148 plasma membrane underlying the cuticular layer (Figs. 2C and S3C-C"). This
149 observation is expected, as the cuticle of extracellular origin is being deposited onto
150 the scale cell membrane. At 52% pupal development, plasma membrane shows
151 distinct pleating corresponding to the developing ridges, with irregular crossribs in
152 between (Figs. 2A'-C', and S4A'-C'). The bulk of cuticle remains above the plasma
153 membrane at this stage (Figs. 2C', and S4C"). At around 62% pupal development,
154 ridges appear to have grown to their near final configuration while lectin staining
155 reveals planar, disk-like cuticular features (hereafter cuticular disks) arranged in rows
156 in between the ridges (Figs. 2A"-C", 2A'"-C'", S5 and S6).
157
158 *Dynamics of F-actin reorganization in Parides eurimedes*
159 We also co-stain chitin and F-actin on the developing pupal scales to
160 investigate the role of cytoskeleton in scale nanostructure formation. Interestingly, as
161 cuticular disks of various sizes are forming in between ridges at 57% development, F-
162 actin bundles are breaking down into short fibrils distributed around the disks (Figs.
163 3B-C, and S7 and movie S1). As the scales became more sclerotized and flattened
164 out later in development (at 67%), disintegrating F-actin appears to reorganize and
165 associate more clearly with cuticular disks, which now appear elongated and slightly
166 tubular in cross-sectional view (Figs. 3A'-C', S8 and movie S2). By 76% development,
167 the cuticular disks appeared hollow, and are surrounded by distinct bulb-like
168 structures formed by the disintegrated F-actin bundles (Figs. 3A"-C", S9 and movie
169 S3).

170 To better understand the mechanism behind F-actin reorganization, we
171 investigated whether the actin-related proteins, Arp2/3 complex, is a potential factor
172 regulating the dendritic growth of actin fibrils (Hudson and Cooley, 2002; Pollard,
173 2007; Rouiller et al., 2008). At around 52% development in *P. eurimedes*, Arp2/3
174 complex appear in a sparse punctate pattern while the F-actin bundles are still intact
175 (Figs. 4A-C, and S10). As F-actin bundles disintegrate and start to reorganize around
176 62% development, a relatively higher density of punctate Arp2/3 complex is seen in
177 close association with the F-actin network (Figs. 4A'-C', and S11). At a later stage
178 (~76% development), no distinctive punctate patterns can be discerned (Figs. 4A"-C",
179 and S12), which is expected given that the reorganization of F-actin is nearly complete
180 by this stage (see Fig. 3). However, the scales are more mature at this point with
181 prominent ridges, and autofluorescence signal from the cuticle has shifted into the
182 green wavelengths (Fig. S13), complicating the interpretation of the Arp2/3
183 immunofluorescence signal.
184
185 *Pharmacological disruption of Arp2/3 using CK-666*
186 In order to mechanistically test the putative role of Arp2/3 in reorganizing F-
187 actin during honeycomb lattice formation, we carried out pharmacological disruption
188 experiments in pupae of both *Parides* and *Papilio* species using CK-666, a known
189 inhibitor of the Arp2/3 complex (Henson et al., 2015). Unfortunately, we were only able
190 to obtain a small number of *Parides* pupae (N = 15), which were already somewhat
191 mature when they arrived, and further, a third of the pupae were dead on arrival (Table
192 S1). Honeycomb lattices can be seen in scales from emerged males of both *P.*
193 *eurimedes* and *P. iphidamas* pupae treated with CK-666 (Fig. S14). However, the
194 height of the honeycombs in scales from pupae treated on 52% development were on

average lower than the control (Figs. S14A and D). Furthermore, in *P. eurimedes*, the height of the honeycombs in scales from pupae injected at 57% development were higher on average than those treated at 52% development, but indistinguishable from any controls (Fig. S14A). These results are reminiscent of a previous study utilizing cytochalasin-D to inhibit linear actin polymerization (Dinwiddie et al., 2014) that found that once the pupae were past a certain developmental stage, ridge formation is no longer disrupted by the inhibitor. However, despite this intriguing trend in our results being consistent with a hypothesized role for Arp2/3, we require data with robust sample sizes and younger time points (*i.e.* 28%-48% development) for *Parides spp.* in future experiments to validate the role of Arp2/3.

We also injected CK-666 into the wing pouches of the more readily available *Papilio polytes* pupae from 40%-80% development to cover the possible timeframe during which Arp2/3 complex could be involved in F-actin reorganization. However, neither cuticular disks nor the dendritic reorganization of linear F-actin bundles are observed in *P. polytes*, whose adult scales have irregular crossribs without the deep lattice walls, *i.e.*, no honeycombs (Fig. S15B and C). Shortly after ridge formation at 60% development (Fig. S15 D-D''), irregular crossribs are seen in between intact F-actin bundles (Fig. S15 F-F''). At 70% development, strong chitin autofluorescence signal is seen at the ridges (Fig. S15 H-I). Since F-actin reorganization is absent in this species, Arp2/3 inhibition did not disrupt ridge and crossrib formation in *P. polytes* as expected (Fig. S16). Concurrent SEM imaging of pupal scales from the same samples show the formation of irregular crossribs is similarly not affected (Fig. S17). Our results suggests the formation of cuticular disks and their subsequent extrusion by reorganizing F-actin is restricted to species with elaborate honeycomb lattice walls such as *Parides eurimedes*.

Honeycomb morphogenesis is conserved across Papilionidae

We also assayed the development of pupal wing scales of several other papilionid species: *Parides arcas*, *Papilio nireus, and Papilio palinurus,* (Fig. 5), Although we were unable to obtain pupae with clearly marked pupation dates for these three species, we observed similar early stages of honeycomb development as seen in *P. eurimedes*. In adult male *P. arcas*, green scales have well developed honeycomb lattice walls that sit above single gyroid crystals (Fig. 5A). During *P. arcas* pupal scale development, both solid and hollow (annular) cuticular disks can be observed in between intact linear actin bundles (Fig. 5B-B' and C-C'). The same is observed in *P. nireus*, where the upper lamina of adult blue scales consists of an elaborate honeycomb lattice with smaller sized pores (Fig. 5D, E and F). In *P. palinurus* adults, green forewing cover scales feature large concave depressions in between the ridges (Fig. 5G). Phalloidin staining of pupal *P. palinurus* scales reveals reorganization of longitudinal F-actin bundles into a shallow concave network (concentric rings in cross-section) (Figs. 5H-I, and Movie S4), which closely correspond to the cuticular dimples seen in adult green cover scales.

Discussion

Swallowtail butterflies (Papilionidae) is the sister lineage to all other butterflies (Espeland et al., 2018) and the showcase family of lepidopterans, as they exhibit some of the most diverse assortment of wing scale nanostructures (Ghiradella, 1985; Prum et al., 2006). Papilionid wing scales generally exhibit irregular crossribs, with some having underlying cuticular walls enclosing tubular pores, although the regularity and depth of the walls vary between species (Fig. S1). These crossrib patterns are unlike

245 the regular, rectilinear crossribs commonly seen in other lepidopteran families, *e.g.*,
246 Nymphalidae (Fig. S1R). In this study, we extended previous observations that
247 parallel F-actin bundles configure the spacing and position of longitudinal ridges of
248 wing scales (Day et al., 2019; Dinwiddie et al., 2014; Ghiradella, 1974; Pomerantz et
249 al., 2020) to Papilionidae, further supporting the hypothesis that this mechanism is
250 broadly conserved across lepidopterans.

251 Our first novel finding is the appearance of irregular crossrib patterns in the
252 plasma membrane between surface ridges, which seemed to serve as a template for
253 chitin accretion into chitinous disks. This process is important as it marks the
254 beginning of honeycomb lattice formation. Further, our results revealed that F-actin
255 plays a predominant and previously unconsidered role in the morphogenesis of some
256 papilionid butterfly wing scales. Once the longitudinal ridges have developed, F-actin
257 bundles, which typically degenerate in nymphalid species (Day et al., 2019; Dinwiddie
258 et al., 2014), subsequently reorganize into a reticulate network surrounding rows of
259 cuticular disks on the scale surface. This actin network likely draws in plasma
260 membrane underlying the cuticular disks into a porous honeycomb lattice. Similar non-
261 linear F-actin morphologies have been observed in other organisms. In diatoms, F-
262 actin organizes into an interdigitating mesh-like porous network during development
263 (Tesson and Hildebrand, 2010). This actin network defines frustule (cell walls)
264 morphogenesis by providing a template for silica biomineralization at the meso and
265 micro scales. In mammalian cells, transient ring-like F-actin structures are thought to
266 drive autophagosome generation by serving as a scaffold for mitophagy initiation
267 structures. 3D-SIM revealed F-actin partially associating with mitochondria in the form
268 of curved sheet (Hsieh and Yang, 2019), akin to the F-actin structures seen in this
269 study.

The schematic in Figure 6 illustrates our proposed formation of honeycomb lattices in some Papilionid wing scales. During early stages of scale formation, F-actin bundles prefigure the loci of future ridge formation in between adjacent actin bundles (Dinwiddie et al., 2014). Plasma membrane then forms a scaffold resembling the irregular crossrib pattern. The cuticle accretes into roughly circular disks delineated by the scaffold. Reorganization of F-actin around the chitinous disks draws the plasma membrane along with the overlying cuticle inwards, moulding it into the lengthened cuticular walls of the honeycomb lattice.

In our attempt to unravel the molecular players in actin reorganization, we used CK-666 to inhibit the role of Arp2/3 complex in actin branching (Henson et al., 2015). However, CK-666 did not quite disrupt the formation of honeycombs even when administered across multiple timepoints. A variety of reasons could potentially explain this. While 100uM of CK-666 has been shown to work in other animal models (Henson et al., 2015), it might still not be a sufficient titre for papilionid butterfly pupal scales. Unfortunately, due to logistical difficulties in obtaining and rearing *Parides spp.*, we were unable to perform a thorough optimization using CK-666. Furthermore, the *Parides* pupae were likely too mature at the time of CK-666 treatment, when the F-actin network has already been established (52% development). In a recent study (Sakamoto et al., 2018), CK-666 did not disrupt the formation of cortical actin meshwork in Sertoli cells of mouse seminiferous tubules, as they were found to be regulated by formins rather than Arp2/3. This suggests that other molecular players, including formins, could be involved in wing scale honeycomb morphogenesis and needs testing.

We note that the irregular crossrib patterns are in place while the ridges are still growing (Fig. 2A'-C'). These crossribs appear to constrain and delineate the

accumulation of cuticle into planar disks in between the ridges. A close examination of SEM images (Figs. 1B and S1) reveals that the endpoints of crossribs at the ridge interface are often connected to microribs present on the ridges. Given their relatively small size and pitch, we are unable to resolve the development of microribs here, which likely requires imaging techniques with even higher resolution such as Photo-activated localization microscopy (PALM) and stochastic optical reconstruction microscopy (STORM). However, both the periodic stripes (microribs) and quasi-periodic spots (crossribs) are reminiscent of Turing patterns (Meinhardt, 1982; Turing, 1952), *i.e.*, implying that an activator-inhibitor type mechanism could be involved in their formation. Alternatively, the crossrib pattern could be produced as a result of spontaneous processes like Ostwald ripening, phase separation, and/or biomechanical forces determined by the mechanical properties of the membranes, leading to stable, quasi-periodic, foam-like perforations on the plasma membrane in between ridges (Dinwiddie et al., 2014; Elson et al., 2010; McDougal et al., 2021; Rosetti et al., 2017; Voorhees, 1985; Wilts et al., 2019).

Overall, the presence of chitinous disks followed by F-actin reorganization appears to be specific to species with extended honeycomb lattice walls, *e.g. Parides eurimedes, Parides arcas*, and *Papilio nireus* (Fig. S1A and S1E). Such reorganized actin structures are not observed in species with shallow irregular crossribs, such as *P. polytes* (Fig. S15). On the other hand, several *Papilio* species (*e.g.*, *palinurus*, *blumei*, *karna*) possess multi-layered cover scales (Ghiradella; Prum et al., 2006; Trzeciak et al., 2012) with widely spaced and reduced (in both height and number) ridges. These scales have no apparent crossribs, trabeculae or honeycombs. Instead, they have a characteristic inter-ridge array of concave depressions and underlying perforated lamellae in the scale interior (Fig. S1L and M). Based on our observations,

320 we speculate that the dimpled appearance of cover scales is templated by
321 reorganization of F-actin bundles into a whorl-like concave network. This could
322 represent an extreme modification of the proposed developmental program of the
323 usual papilionid honeycomb lattice. Without crossribs, the pore sizes of honeycombs
324 are likely constrained only by the pitch of the ridges. This is consistent with our
325 observation that the outermost F-actin rings possess dimensions approaching the
326 inter-ridge distance (Fig. 5C). Without the trabeculae, the lumen multilayer fills the
327 entire interior of the scale right up to the shallow dimples.

328 Interestingly, in typical lepidopteran scale cells, the trabeculae extend
329 downwards from the crossribs and form columns of arches in between the ridges
330 (Ghiradella, 1974; Ghiradella, 1985; Ghiradella, 1989; Ghiradella and Radigan, 1976;
331 Overton 1966), suggesting they are developmentally connected. Recently, Matsuoka
332 and Monteiro (2018) found that *DDC* mutant of *Bicyclus anynana* (Nymphalidae)
333 possessed irregularly-spaced and thin crossribs with sheet-like vertical trabeculae
334 instead of feet-like, arched trabeculae (see Fig. 4A of (Matsuoka and Monteiro, 2018)).
335 These mutant scale morphologies are somewhat reminiscent of the irregular crossribs
336 and honeycomb lattice walls of Papilionidae. This suggests spatio-temporal changes
337 in expression patterns of single genes such as *DDC* could possibly alter crossrib
338 morphology and drive honeycomb formation. However, any putative pleiotropic role of
339 pigment-pathway genes in organizing papilionid scale morphology should be
340 reconciled with that of actin reorganization. Future studies could look at knocking out
341 *DDC* and other pigment-pathway genes during papilionid pupal development, in
342 addition to inhibiting actin-binding proteins including Arp2/3 and formins, and tinkering
343 with master regulatory genes like *optix* (Banerjee et al., 2022; Wasik et al., 2014;
344 Zhang et al., 2017b).

The smooth endoplasmic reticulum (SER) has been implicated in templating luminal scale nanostructures during pupal development. Given that the papilionid honeycomb lattice extends into the lumen of the scale cells, any putative role of the SER in honeycomb morphogenesis should also be investigated. It would be of interest to follow the development of pupal wing scales using tissue clearing techniques or attempt a more finely resolved developmental time series to capture the full complexity of molecular and cytoskeletal dynamics. Comparatively understanding the morphogenesis of hierarchical nanostructures across biodiversity could inspire facile, biomimetic routes to synthesizing hierarchically structured materials for technological applications, given current challenges in the engineering of complex multi-functional mesophases (Kolle et al., 2010; Pokroy et al., 2009; Potyrailo et al., 2007; Siddique et al., 2017).

Materials and Methods

Experimental design

To understand the process of scale nanostructure formation, we performed time-resolved imaging on developing pupal scales using specific biomarkers conjugated with fluorophores. Since cellular membranes and cytoskeletal elements have been identified as key components driving scale cell development, we used biomarkers targeting F-actin, cuticle (chitin), plasma membrane and Arp2/3 complex. We used 3D structured illumination microscope (3D-SIM) and lattice SIM to try and resolve structures beyond the diffraction limit. We would have preferred to present all confocal and SIM data solely on a single patch, for instance, the green dorsal forewing cover scales of pupal *P. eurimedes*. However, for time points where scales were highly

370 crumpled or folded, we addressed this gap with data from black areas adjacent to the
371 green patch, or from homologous yellow dorsal forewing patch on females. The overall
372 consistency of the results validates our approach.
373
374 *Dissection of pupae and tissue preparation*
375 Pupae were purchased in multiple batches from Marl Insect and Butterfly Culture
376 (Philippines), Stratford-upon-Avon Butterfly Farm (UK), and Mariposario del Bosque
377 Nuevo (Costa Rica) between June 2017 - April 2021. Precise pupation dates were
378 only available for *Papilio polytes* and one batch of *P. eurimedes* pupae. For *Parides*
379 batches without information on the pupation dates, we were able to estimate the rough
380 pupation stage (indicated by ~, *e.g.*, Figs. 2A'''-C''', and 4) by morphological
381 comparisons to this reference *P. eurimedes* batch. Sex of each pupa was determined
382 by examining markings on the ventral segments. Wings from each pupa were
383 dissected in cold Phosphate Buffer Saline (PBS) and immediately fixed in 4% PEM-
384 PFA at room temperature for 15 mins. Following washes in PBS, wings were placed
385 in blocking buffer (0.5% NP-40) at 4ºC overnight prior to staining. The average
386 duration from pupation to emergence is 10 days for *P. polytes* and 21 days for *P.*
387 *eurimedes*. We report the percentage of development in our time series for ease of
388 comparison between species with different developmental rates.
389
390 *Developmental time series with Wheat Germ agglutinin, phalloidin and anti-Arp2*
391 Wheat Germ Agglutinin (WGA) was previously used to visualize butterfly scale cell
392 growth and is thought to initially stain plasma membrane before switching to chitin at
393 later developmental stages (Dinwiddie et al., 2014). Phalloidin is a standard method
394 to visualize F-actin. For AF-555 WGA and AF-647 phalloidin double-staining, pupal

395 wings were incubated in 1:200 dilution of Alexa Fluor 555-conjugated WGA (Invitrogen
396 W32464) and 1:40 dilution of Alexa Fluor 647-conjugated phalloidin (Invitrogen
397 A22287) for an hour at room temperature. For FITC WGA and TRITC phalloidin
398 double staining, *P. palinurus* pupal wings were incubated in 1:100 dilution of FITC
399 WGA (EY Labs F-2101-5) and 1:100 dilution of TRITC phalloidin (Sigma P1951) for
400 an hour at room temperature. Arp2 is the ATP-binding component of the actin Arp2/3
401 complex, which functions as an actin nucleator in branched actin networks (Goley and
402 Welch, 2006; Smith et al., 2013). After blocking, pupal wings were incubated with a
403 1:500 dilution of rabbit anti-Arp2 (Abcam ab47654; pblast search revealed Uniprot
404 #P61160, Human Arp2 has 82% sequence similarity to XP_013178655.1, *Papilio*
405 *xuthus Arp2*) at 4℃ overnight. After washing, the wings were incubated in buffer with
406 a 1:300 dilution of Alexa Fluor 594 Goat anti Rabbit secondary antibody (Abcam
407 ab150088) for an hour at room temperature.
408
409 *Time series with CellMask Plasma Membrane stain*
410 As the CellMask plasma membrane stain does not survive permeabilization, dissected
411 pupal wings were immediately stained with a 1:300 dilution of CellMask Deep Red
412 (Invitrogen C10046) for 10 mins. After removing the staining solution, the wings were
413 fixed in 4% PEM-PFA at room temperature for 15 mins. Following washes in PBS,
414 pupal wings were stained with a 1:200 dilution of Alexa Fluor 555-conjugated WGA
415 (Invitrogen W32464) for an hour at room temperature. In order to prevent
416 permeabilization, the buffers for Cellmask stains did not contain any detergents (e.g.
417 Triton).
418
419

420 *Arp2/3 inhibition with CK-666*

421 CK-666 was purchased from Sigma Aldrich (SML0006) and the stock solution was
422 dissolved in DMSO. For pupal injections, CK-666 was diluted in 1x Grace's insect
423 medium to final concentration of 100μM. Two to three P. polytes pupae were injected
424 with CK-666 at 40%, 50%, 60%, 70%, and 80% development. Around 8-10μL of CK-
425 666 is injected into wing pouches using a glass needle. Control pupae were injected
426 with equal volume of DMSO diluted in Grace's insect medium. All injected pupae were
427 dissected at 80% development and stained for immunofluorescence. Pupae injected
428 on 80% development were allowed to develop for at least two hours before dissection.

429

430 *Negative controls*

431 For experiments with non-fluorophore-conjugated primary antibodies (Arp2 staining),
432 we labelled a separate wing from the same individual with the secondary antibody
433 only. This is to determine if the observed fluorescence signal is due to non-specific
434 binding of secondary antibodies. After blocking, pupal wings were incubated without
435 primary antibodies (only buffer) at 4℃ overnight. After washing, the wings were
436 incubated with a 1:300 dilution of Alexa Fluor 594 Goat anti Rabbit secondary antibody
437 (Abcam ab150088) for an hour at room temperature. Negative controls were imaged
438 using the same settings (laser power, gain, *etc*.) as the anti-*Arp2* antibody-stained test
439 samples.

440

441 *Image acquisition, data processing*

442 Following washes, the wings were mounted on glass slides in Prolong Gold antifade
443 (Life Technologies P36930), covered with #1 thickness coverslips and sealed with nail
444 polish. Confocal images were acquired using Olympus FV3000 (60x), Nikon A1R

445 (100x) and Leica SP8 (100x). 3D-SIM was performed on a DeltaVision OMX and
446 lattice SIM using Zeiss Elyra 7. Confocal data acquired with Olympus FV3000 and
447 Nikon A1RSIM data were deconvolved using default settings in Huygens Professional
448 v20.04. Confocal data acquired with Leica SP8 were deconvolved using default
449 settings in Leica's Lightning deconvolution software during acquisition. All images
450 were examined and processed using Bitplane Imaris Viewer 9.5.1. Movies were
451 generated using Bitplane Imaris and edited using Shotcut v19.07.15 (Meltytech, LLC)
452
453 *Critical point drying (CPD)*
454 Wings from each pupa were dissected in cold PBS and immediately fixed in 4% PEM-
455 PFA at room temperature for 15 mins. Following washes in PBS, wings were
456 subjected to serial dehydration in 25%, 50%, 70%, 90% and absolute ethanol for 10
457 minutes each. The specimens were then transferred to the sample holders and dried
458 using Leica EM CPD300 Automated Critical Point Dryer with the following settings:
459 (CO2 influx) Medium speed, 120s delay; (Exchange process) Speed 5, 14 cycles;
460 Medium heating speed; and Medium gas out speed. It should be note that direct air
461 drying of soft samples *e.g.* pupal wing scales is not recommended, as water surface
462 tension forces will result in significant distortion of specimen structure (Bray et al.,
463 1993).
464
465 *Conventional and focused ion beam (FIB) scanning electron microscopy (SEM)*
466 Adult scales were individually picked with a needle and placed on carbon tape.
467 Mounted scales were fractured using a razor-blade to obtain cross-sectional views.
468 All samples were sputter-coated with platinum or gold to increase conductivity and

reduce charging. Samples were imaged using JEOL JSM 6010LV Scanning Electron Microscope at 15-20k.

For focused ion beam (FIB) milling, samples were prepared by sputter-coating with platinum to increase conductivity. The sectioned scale shown in Fig. 1C is milled using a gallium ion beam on a FEI Versa 3D with the following settings: beam voltage - 8kV, beam current - 12pA at a 52° tilt. Image acquisition was performed in the same equipment with the following settings: beam voltage - 5kV, beam current - 13pA.

Acknowledgements:

We are indebted to Antonia Monteiro for generously providing us with lab resources, including the use of insectary. We thank Cédric Finet for sharing FIB-SEM image of *P. eurimedes*. We are grateful to the Monteiro lab, C. Finet, Cynthia He, Rong Li, Sasha Bershadsky, and Dan Morse for their thoughtful suggestions. We thank Sree Vaishnavi Sundararajan and Gianluca Grenci (MBI) for access and help with SEM, Tong Yan (CBIS), Mak Kah Jun and Peng Qiwen (MBI), Laura and Keshmarathy Sacadevan (Singhealth Advanced Bioimaging) for help with confocal microscopy, Graham Wright and Goh Wah Ing (A*STAR AMP) and Shi Xianke (Zeiss) for help with SIM data acquisition.

Funding: This work was supported by a Graduate Research Excellence Grant - Rosemary Grant Advanced Award from SSE to K.S., Yale-NUS startup funds (R-607-261-182-121) and a Singapore NRF CRP Award (CRP20-2017-0004) to V.S.

Author Contributions: V.S. and K.S. designed the study. K.S. performed the experiments. Both authors analyzed the results and wrote the manuscript.

Competing interests: Authors declare no competing interests.

498 **References**

499 **Banerjee, T. D., Kwi-Shan, S. and Monteiro, A.** (2022). Reuse of a wing
500 venation gene-regulatory network in patterning the eyespot rings of butterflies.
501 *BioRxiv*, 2021.05.22.445259.

502 **Beldade, P. and Brakefield, P. M.** (2002). The genetics and evo-devo of
503 butterfly wing patterns. *Nat Rev Genet* **3**, 442-52.

504 **Bray, D. F., Bagu, J. and Koegler, P.** (1993). Comparison of
505 hexamethyldisilazane (HMDS), Peldri II, and critical-point drying methods for
506 scanning electron microscopy of biological specimens. *Microsc Res Tech* **26**, 489-
507 495.

508 **Brien, M. N., Enciso-Romero, J., Lloyd, V. J., Curran, E. V., Parnell, A. J.,**
509 **Morochz, C., Salazar, P. A., Rastas, P., Zinn, T. and Nadeau, N. J.** (2022). The
510 genetic basis of structural colour variation in mimetic Heliconius butterflies. *Philos*
511 *Trans R Soc Lond B Biol Sci* **377**, 20200505.

512 **Day, C. R., Hanly, J. J., Ren, A. and Martin, A.** (2019). Sub-micrometer
513 insights into the cytoskeletal dynamics and ultrastructural diversity of butterfly wing
514 scales. *Developmental Dynamics* **248**, 657-670.

515 **Dinwiddie, A., Null, R., Pizzano, M., Chuong, L., Leigh Krup, A., Ee Tan,**
516 **H. and Patel, N. H.** (2014). Dynamics of F-actin prefigure the structure of butterfly
517 wing scales. *Dev Biol* **392**, 404-18.

518 **Elson, E. L., Fried, E., Dolbow, J. E. and Genin, G. M.** (2010). Phase
519 Separation in Biological Membranes: Integration of Theory and Experiment. *Annual*
520 *Review of Biophysics* **39**, 207-226.

521 **Espeland, M., Breinholt, J., Willmott, K. R., Warren, A. D., Vila, R.,**
522 **Toussaint, E. F. A., Maunsell, S. C., Aduse-Poku, K., Talavera, G., Eastwood, R.**

523 **et al.** (2018). A Comprehensive and Dated Phylogenomic Analysis of Butterflies.
524 *Current Biology* **28**, 770-778.e5.
525 **Ficarrotta, V., Hanly, J. J., Loh, L. S., Francescutti, C. M., Ren, A.,**
526 **Tunstrom, K., Wheat, C. W., Porter, A. H., Counterman, B. A. and Martin, A.**
527 (2022). A genetic switch for male UV iridescence in an incipient species pair of
528 sulphur butterflies. *Proc Natl Acad Sci U S A* **119**.
529 **Ghiradella, H.** (1974). Development of ultraviolet-reflecting butterfly scales:
530 How to make an interference filter. *Journal of Morphology* **142**, 395-410.
531 **Ghiradella, H.** (1984). Structure of Iridescent Lepidopteran Scales -
532 Variations on Several Themes. *Annals of the Entomological Society of America* **77**,
533 637-645.
534 **Ghiradella, H.** (1985). Structure and development of iridescent lepidopteran
535 scales: the Papilionidae as a showcase family. *Annals of the Entomological Society*
536 *of America* **78**, 252-264.
537 **Ghiradella, H.** (1989). Structure and development of iridescent butterfly
538 scales: Lattices and laminae. *Journal of Morphology* **202**, 69-88.
539 **Ghiradella, H. and Radigan, W.** (1976). Development of butterfly scales. II.
540 Struts, lattices and surface tension. *J Morphol* **150**, 279-297.
541 **Goley, E. D. and Welch, M. D.** (2006). The ARP2/3 complex: an actin
542 nucleator comes of age. *Nature reviews. Molecular cell biology* **7**, 713-26.
543 **Henson, J. H., Yeterian, M., Weeks, R. M., Medrano, A. E., Brown, B. L.,**
544 **Geist, H. L., Pais, M. D., Oldenbourg, R. and Shuster, C. B.** (2015). Arp2/3
545 complex inhibition radically alters lamellipodial actin architecture, suspended cell
546 shape, and the cell spreading process. *Molecular Biology of the Cell* **26**, 887-900.

547 **Hsieh, C. W. and Yang, W. Y.** (2019). Omegasome-proximal PtdIns(4,5)P(2)
548 couples F-actin mediated mitoaggregate disassembly with autophagosome
549 formation during mitophagy. *Nat Commun* **10**, 969.
550 **Hudson, A. M. and Cooley, L.** (2002). A subset of dynamic actin
551 rearrangements in Drosophila requires the Arp2/3 complex. *J Cell Biol* **156**, 677-87.
552 **Kolle, M., Salgard-Cunha, P. M., Scherer, M. R. J., Huang, F. M., Vukusic,**
553 **P., Mahajan, S., Baumberg, J. J. and Steiner, U.** (2010). Mimicking the colourful
554 wing scale structure of the Papilio blumei butterfly. *Nature Nanotechnology* **5**, 511-
555 515.
556 **Matsuoka, Y. and Monteiro, A.** (2018). Melanin Pathway Genes Regulate
557 Color and Morphology of Butterfly Wing Scales. *Cell Rep* **24**, 56-65.
558 **McDougal, A., Miller, B., Singh, M. and Kolle, M.** (2019). Biological growth
559 and synthetic fabrication of structurally colored materials. *Journal of Optics* **21**,
560 073001.
561 **McDougal, A. D., Kang, S., Yaqoob, Z., So, P. T. C. and Kolle, M.** (2021).
562 In vivo visualization of butterfly scale cell morphogenesis in Vanessa cardui. *Proc*
563 *Natl Acad Sci U S A* **118**, e2112009118.
564 **Meinhardt, H.** (1982). Models of Biological Pattern Formation. London:
565 Academic Press.
566 **Nadeau, N. J., Pardo-Diaz, C., Whibley, A., Supple, M. A., Saenko, S. V.,**
567 **Wallbank, R. W. R., Wu, G. C., Maroja, L., Ferguson, L., Hanly, J. J. et al.** (2016).
568 The gene cortex controls mimicry and crypsis in butterflies and moths. *Nature* **534**,
569 106-110.
570 **Nishikawa, H., Iijima, T., Kajitani, R., Yamaguchi, J., Ando, T., Suzuki, Y.,**
571 **Sugano, S., Fujiyama, A., Kosugi, S., Hirakawa, H. et al.** (2015). A genetic

572 mechanism for female-limited Batesian mimicry in Papilio butterfly. *Nat Genet* **47**,
573 405-409.
574 **Overton , J.** (1966). Microtubules and microfibrils in morphogenesis of the
575 scale cells of Ephestia kühniella. *Journal of Cell Biology* **29**, 293-305.
576 **Pokroy, B., Kang, S. H., Mahadevan, L. and Aizenberg, J.** (2009). Self-
577 organization of a mesoscale bristle into ordered, hierarchical helical assemblies.
578 *Science* **323**, 237-40.
579 **Pollard, T. D.** (2007). Regulation of Actin Filament Assembly by Arp2/3
580 Complex and Formins. *Annual Review of Biophysics and Biomolecular Structure* **36**,
581 451-477.
582 **Pomerantz, A. F., Siddique, R. H., Cash, E. I., Kishi, Y., Pinna, C.,**
583 **Hammar, K., Gomez, D., Elias, M. and Patel, N. H.** (2020). Developmental,
584 cellular, and biochemical basis of transparency in the glasswing butterfly Greta oto.
585 *BioRxiv*, 2020.07.02.183590.
586 **Potyrailo, R. A., Ghiradella, H., Vertiatchikh, A., Dovidenko, K.,**
587 **Cournoyer, J. R. and Olson, E.** (2007). Morpho butterfly wing scales demonstrate
588 highly selective vapour response. *Nat Photon* **1**, 123-128.
589 **Prakash, A., Finet, C., Banerjee, T. D., Saranathan, V. and Monteiro, A.**
590 (2022). Antennapedia and optix regulate metallic silver wing scale development and
591 cell shape in Bicyclus anynana butterflies. *Cell Rep* **40**, 111052.
592 **Prakash, A., Finet, C., Saranathan, V. and Monteiro, A.** (2021).
593 Antennapedia regulates metallic silver wing scale development and cell shape in
594 Bicyclus anynana butterflies. *BioRxiv*, 2021.10.19.46493.

595 **Prum, R. O., Quinn, T. and Torres, R. H.** (2006). Anatomically diverse
596 butterfly scales all produce structural colours by coherent scattering. *Journal of*
597 *Experimental Biology* **209**, 749-765.
598 **Reed, R. D., Papa, R., Martin, A., Hines, H. M., Counterman, B. A., Pardo-**
599 **Diaz, C., Jiggins, C. D., Chamberlain, N. L., Kronforst, M. R., Chen, R. et al.**
600 (2011). optix Drives the Repeated Convergent Evolution of Butterfly Wing Pattern
601 Mimicry. *Science* **333**, 1137-1141.
602 **Rosetti, C. M., Mangiarotti, A. and Wilke, N.** (2017). Sizes of lipid domains:
603 What do we know from artificial lipid membranes? What are the possible shared
604 features with membrane rafts in cells? *Biochimica et Biophysica Acta (BBA) -*
605 *Biomembranes* **1859**, 789-802.
606 **Rouiller , I., Xu , X.-P., Amann , K. J., Egile , C., Nickell , S., Nicastro , D.,**
607 **Li , R., Pollard , T. D., Volkmann , N. and Hanein , D.** (2008). The structural basis
608 of actin filament branching by the Arp2/3 complex. *Journal of Cell Biology* **180**, 887-
609 895.
610 **Sakamoto, S., Thumkeo, D., Ohta, H., Zhang, Z., Huang, S.,**
611 **Kanchanawong, P., Fuu, T., Watanabe, S., Shimada, K., Fujihara, Y. et al.**
612 (2018). mDia1/3 generate cortical F-actin meshwork in Sertoli cells that is
613 continuous with contractile F-actin bundles and indispensable for spermatogenesis
614 and male fertility. *PLoS Biol.* **16**, e2004874.
615 **Saranathan, V., Osuji, C. O., Mochrie, S. G. J., Noh, H., Narayanan, S.,**
616 **Sandy, A., Dufresne, E. R. and Prum, R. O.** (2010). Structure, function, and self-
617 assembly of single network gyroid (I4(1)32) photonic crystals in butterfly wing scales.
618 *Proceedings Of The National Academy Of Sciences Of The United States Of*
619 *America* **107**, 11676-11681.

Siddique, R. H., Donie, Y. J., Gomard, G., Yalamanchili, S., Merdzhanova, T., Lemmer, U. and Hölscher, H. (2017). Bioinspired phase-separated disordered nanostructures for thin photovoltaic absorbers. *Science Advances* **3**, e1700232.

Smith, B. A., Daugherty-Clarke, K., Goode, B. L. and Gelles, J. (2013). Pathway of actin filament branch formation by Arp2/3 complex revealed by single-molecule imaging. *Proc Natl Acad Sci U S A* **110**, 1285-90.

Sweeney, A., Jiggins, C. and Johnsen, S. (2003). Insect communication: Polarized light as a butterfly mating signal. *Nature* **423**, 31-32.

Tesson, B. and Hildebrand, M. (2010). Extensive and intimate association of the cytoskeleton with forming silica in diatoms: control over patterning on the meso- and micro-scale. *PLoS One* **5**, e14300.

Trzeciak, T. M., Wilts, B. D., Stavenga, D. G. and Vukusic, P. (2012). Variable multilayer reflection together with long-pass filtering pigment determines the wing coloration of papilionid butterflies of the nireus group. *Opt Express* **20**, 8877-90.

Tsai, C. C., Childers, R. A., Nan Shi, N., Ren, C., Pelaez, J. N., Bernard, G. D., Pierce, N. E. and Yu, N. (2020). Physical and behavioral adaptations to prevent overheating of the living wings of butterflies. *Nat Commun* **11**, 551.

Turing, A. M. (1952). The chemical basis of morphogenesis. *Philosophical Transactions of the Royal Society of London* **237**, 37-72.

Van Belleghem, S. M., Ruggieri, A. A., Concha, C., Livraghi, L., Hebberecht, L., Rivera, E. S., Ogilvie, J. G., Hanly, J. J., Warren, I. A., Planas, S. et al. (2023). High level of novelty under the hood of convergent evolution. *Science* **379**, 1043-1049.

Voorhees, P. W. (1985). The theory of Ostwald ripening. *Journal of Statistical Physics* **38**, 231-252.

Wasik, B. R., Liew, S. F., Lilien, D. A., Dinwiddie, A. J., Noh, H., Cao, H. and Monteiro, A. (2014). Artificial selection for structural color on butterfly wings and comparison with natural evolution. *Proceedings Of The National Academy Of Sciences Of The United States Of America* **111**, 12109-12114.

Wee, J. L. Q., Das Banerjee, T., Prakash, A., Seah, K. S. and Monteiro, A. (2022). Distal-less and spalt are distal organisers of pierid wing patterns. *EvoDevo* **13**, 12.

Wilts, B. D., Clode, P. L., Patel, N. H. and Schröder-Turk, G. E. (2019). Nature's functional nanomaterials: Growth or self-assembly? *Mrs Bulletin* **44**, 106-112.

Wilts, B. D., Michielsen, K., De Raedt, H. and Stavenga, D. G. (2012). Iridescence and spectral filtering of the gyroid-type photonic crystals in Parides sesostris wing scales. *Interface Focus* **2**, 681-7.

Wilts, B. D., N, I. and Stavenga, D. G. (2014). Pigmentary and photonic coloration mechanisms reveal taxonomic relationships of the Cattlehearts (Lepidoptera: Papilionidae: Parides). *Bmc Evolutionary Biology* **14**, 160.

Yoda, S., Sakakura, K., Kitamura, T., KonDo, Y., Sato, K., Ohnuki, R., Someya, I., Komata, S., Kojima, T., Yoshioka, S. et al. (2021). Genetic switch in UV response of mimicry-related pale-yellow colors in Batesian mimic butterfly, Papilio polytes. *Sci Adv* **7**, eabd6475.

Zhang, L., Martin, A., Perry, M. W., van der Burg, K. R., Matsuoka, Y., Monteiro, A. and Reed, R. D. (2017a). Genetic Basis of Melanin Pigmentation in Butterfly Wings. *Genetics* **205**, 1537-1550.

669 **Zhang, L., Mazo-Vargas, A. and Reed, R. D.** (2017b). Single master
670 regulatory gene coordinates the evolution and development of butterfly color and
671 iridescence. *Proc Natl Acad Sci U S A* **114**, 10707-10712.

672

673 **Figure 1.** Hierarchical nanostructure of wing scales in *Parides eurimedes*
674 (Papilionidae). (A) Adult male with structurally-colored green patches on their dorsal
675 forewings. Credit: iDigBio YPM Ent 433579. (B) SEM top-view and (C) FIB-SEM
676 cross-sectional image of an adult green scale showing ridges and honeycomb lattice
677 ending in trabeculae on top of a perforated multilayer lattice. Scale bars: (A) – 1cm,
678 (B and C) – 1μm.
679
680 **Figure 2.** Morphogenetic time series of the development of cuticular disks in pupal *P.*
681 *eurimedes* dorsal forewing scales, acquired with a 100x confocal microscope. AF-555
682 WGA (green) stains chitin and Cellmask (red) stains plasma membrane. By 52%
683 development, Hollow vein-like crossribs appear on plasma membrane in between
684 ridges that serve as a scaffold for cuticle accretion. As scales mature, more cuticle is
685 deposited into these rows of disks bounded by plasma membrane. See also Figs. S4-
686 S6. (B-B''') Close up views of A-A'''. (C-C''') *xz* cross-sections of the scale at locations
687 marked with grey lines in A-A''' reveal the planar aspect of the cuticular disks. Yellow
688 ROI in C'-C''' correspond to those in B'-B'''. Scale bars (A-A''') – 5μm, (B-B''' and C-
689 C''') – 2μm.
690
691 **Figure 3.** Morphogenetic time series of the development of columnar honeycomb
692 lattice in pupal *P. eurimedes* dorsal forewing scale cells acquired with super-resolution
693 lattice SIM. AF-555 WGA (green) stains chitin and AF-647 phalloidin (red) stains F-
694 actin. AF-555 WGA show a gradual evolution of the cuticular disks from filled-in planar
695 to hollow tubular outgrowths. The disintegrating F-actin bundles show evidence of
696 reorganization from linear to reticulated features with ring-like cross-sections. See
697 also Figs. S7-S9. (B-B'') Close up views of A-A''. Insets correspond to the regions of

698 interest (ROI) marked in yellow shown with a 3D aspect. (C-C") *xz* cross-sections of
699 the scale at locations marked with grey lines in A-A". Scale bars (A-A") – 5μm, (B-B",
700 C-C" and insets) – 1μm.
701
702 **Figure 4.** Arp2/3 complex is involved in F-actin reorganization in pupal *P. eurimedes*
703 wing scales. Dorsal forewing scales stained with AF-594 anti-Arp2 (green) and AF-
704 647 phalloidin (red) acquired with 100x confocal microscope. Initially (~52%
705 development), Arp2/3 complex appear as sparse punctate dots while the F-actin
706 bundles are still intact. As F-actin bundles disintegrate and reorganize, a relatively
707 higher density of punctate Arp2/3 signal is seen in close association with the reticulate
708 F-actin network. Our oldest timepoint in *P. eurimedes* (~76% development) has a
709 large amount of cuticle autofluorescence overlapping with the AF594 signal, but the
710 punctate pattern can be still discerned. See also Figs. S10-S12. (B-B") Close up views
711 of A-A". (C-C") *xz* cross-sections of the scale at locations marked with grey lines in A-
712 A". Yellow ROIs correspond to those in B-B". Scale bars (A-A") – 5μm, (B-B" and C-
713 C") – 2μm.
714
715 **Figure 5.** Conservation of honeycomb lattice development in genus Parides. SEM
716 cross-section view of (A) adult green scales in *P. arcas,* (D) blue scales in *P.nireus,*
717 and (G) green scales in *P.palinurus.* All pupal dorsal forewing scales are stained either
718 with AF-555 WGA or FITC-WGA (green) showing chitin, and AF-647 phalloidin or
719 TRITC-phalloidin (red) showing F-actin. (B-C) Maximum projected 3D-SIM
720 micrograph of green cover scales in pupal male *P. arcas* featuring planar cuticular
721 disks similar in shape and arrangement to *P. eurimedes*. (B'-C') Maximum projected
722 3D-SIM micrograph of green cover scales of a different male *P. arcas* pupa showing

723 irregular crossribs patterns. (E-F) Maximum projected 3D-SIM micrograph of blue
724 cover scales of pupal *P. nireus*, similarly with crossribs and intact linear actin bundles.
725 (H-I) 60x confocal micrographs of green cover scales of pupal *P. palinurus* shown at
726 two different z-planes. A concave network of F-actin underlie the cuticular dimples. At
727 lower *z*, the actin rings (in cross-section) are smaller in size and show a foam-like
728 appearance. (C-C', F, and I) *xz* cross-sections of the scales with ROI at locations
729 marked with grey lines in B-B', E, and H respectively. Scale bars (A, D, and G) – 5μm,
730 (B-B', C-C', E, and F) – 1μm, (H-I) – 5μm.
731
732 **Figure 6**. A schematic illustrating the proposed morphogenesis of honeycomb lattices
733 in papilionid wing scales. During early stages, F-actin bundles prefigure the loci where
734 ridges form in between adjacent actin bundles. Next the plasma membrane (black
735 lines) forms a scaffold where cuticle (green lines and structures) accumulates into the
736 spaces and forms irregular disk-like structures. Reorganization of F-actin around the
737 disks subsequently extrudes the plasma membrane along with the deposited cuticle,
738 forming the honeycomb lattice walls.

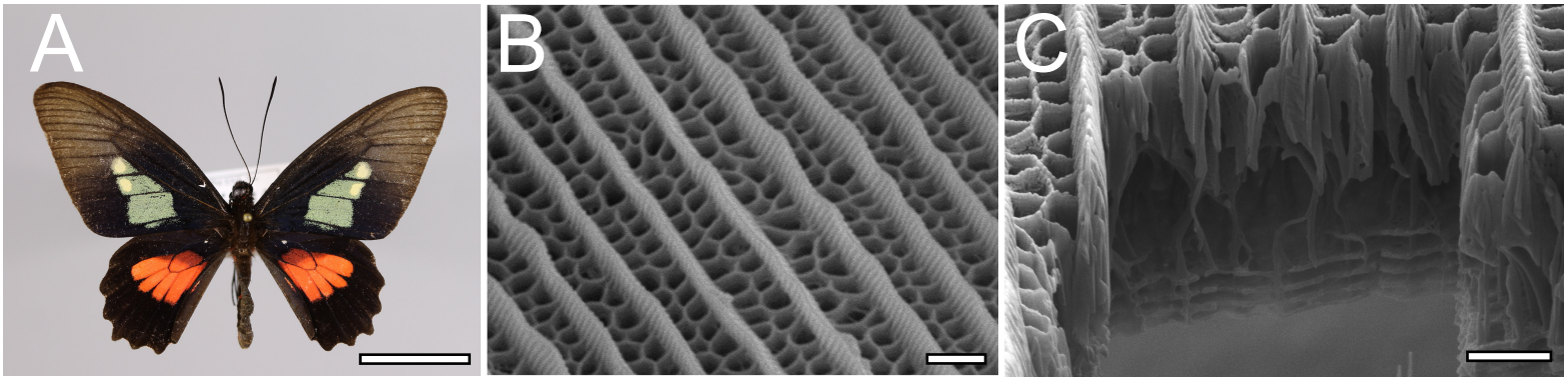
A
B
C

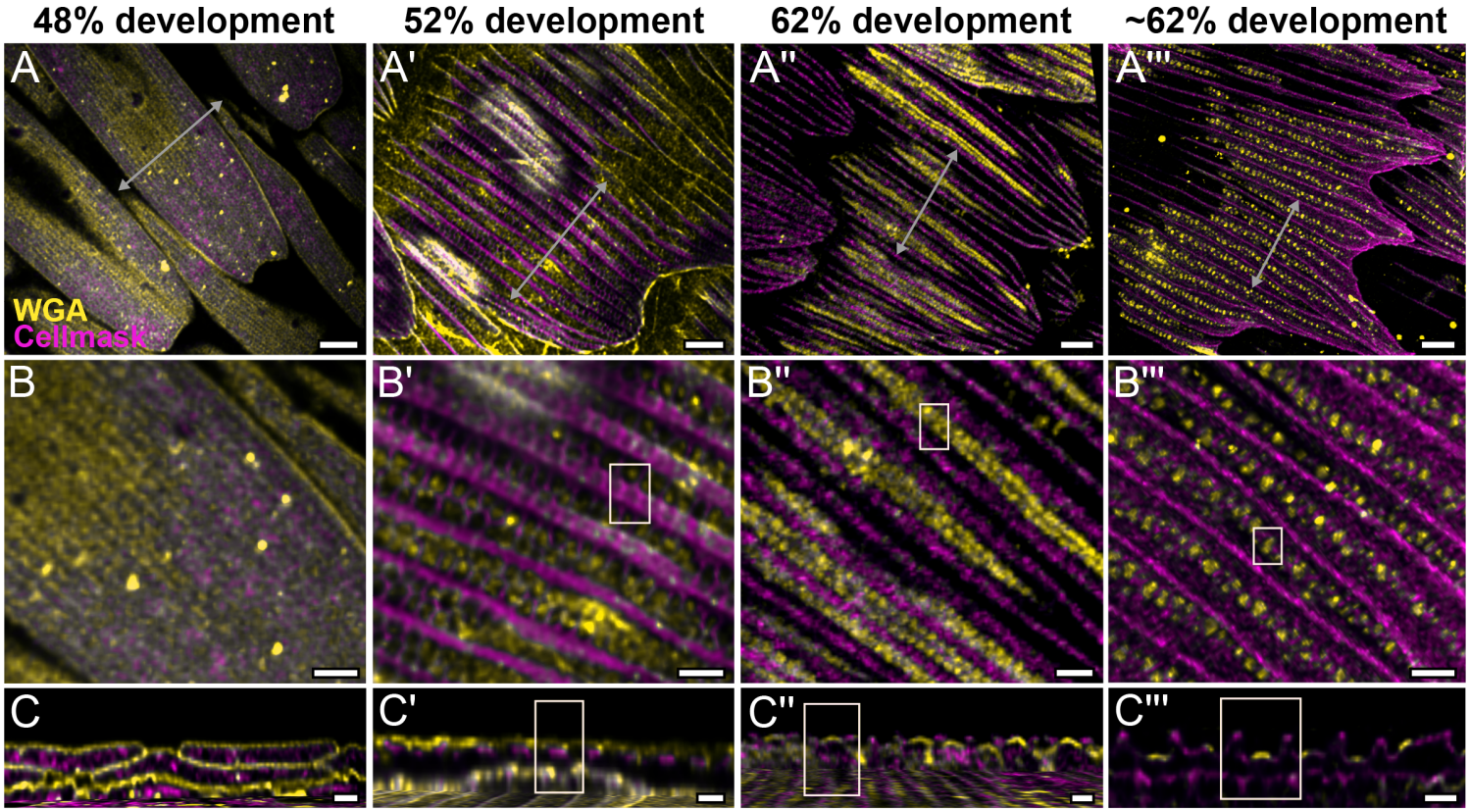
48% development
52% development
62% development
~62% development
A
A'
A''
A'''
WGA
Cellmask
B
B'
B''
B'''
C
C'
C''
C'''

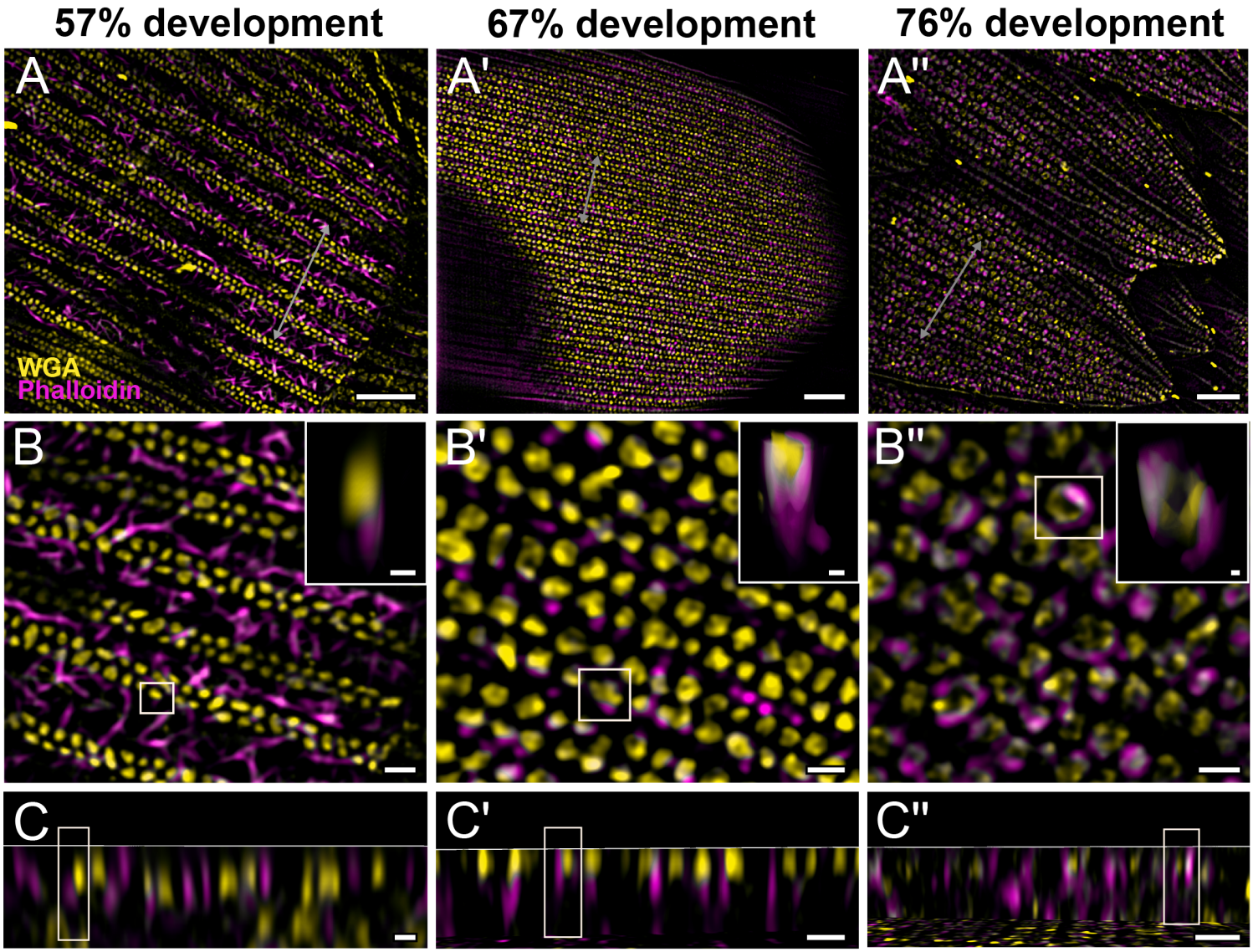
57% development
67% development
76% development
A
A'
A''
WGA
Phalloidin
B
B'
B''
C
C'
C''

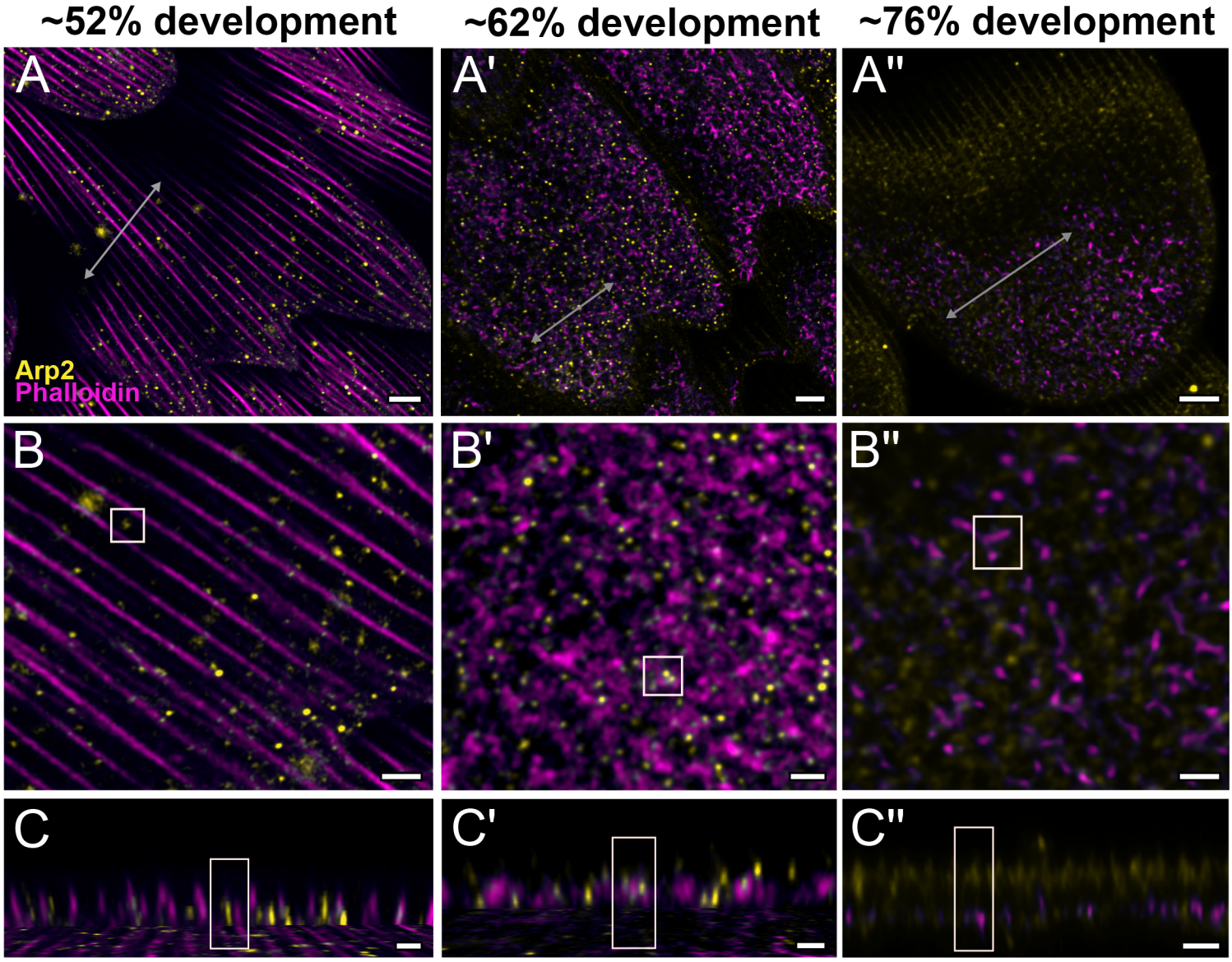
~52% development
~62% development
~76% development
A
A'
A''
Arp2
Phalloidin
B
B'
B''
C
C'
C''

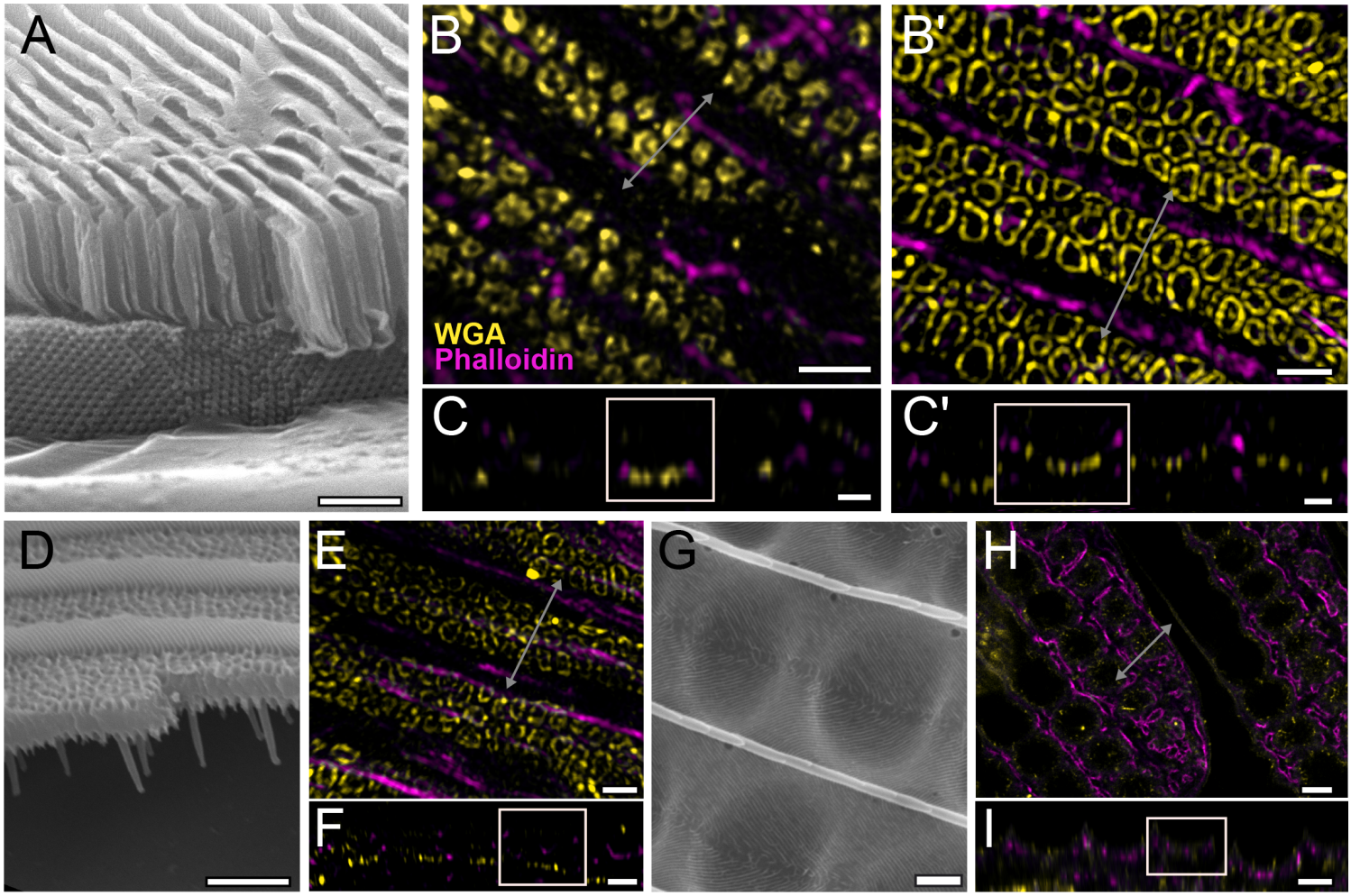
A
B
WGA
Phalloidin
B'
C
C'
D
E
F
G
H
I

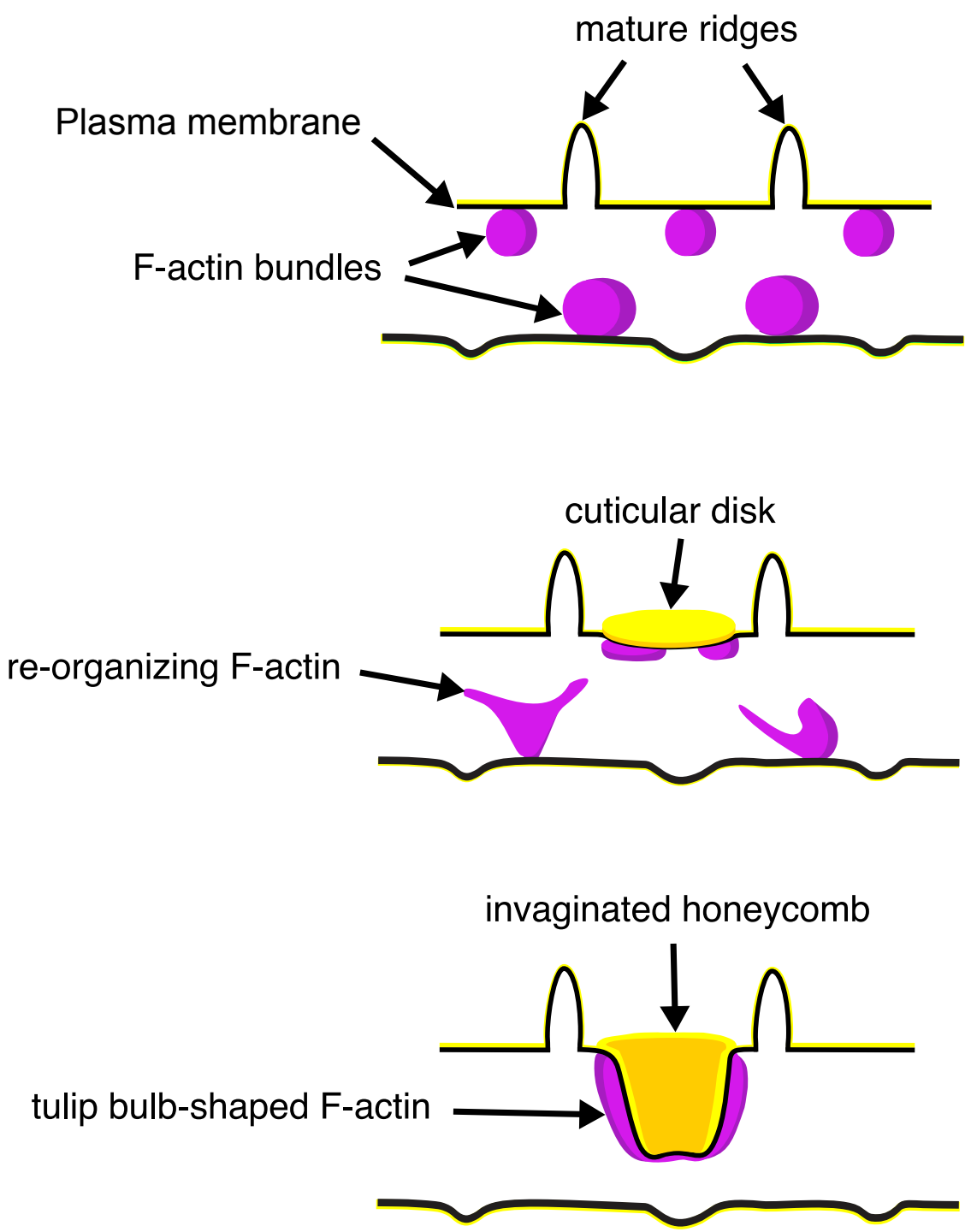
mature ridges
Plasma membrane
F-actin bundles
cuticular disk
re-organizing F-actin
invaginated honeycomb
tulip bulb-shaped F-actin